Marine Structures 33 (2013) 1–20

Contents lists available at SciVerse ScienceDirect

Marine Structures

journal homepage: www.elsevier.com/locate/marstruc

Optimization of composite catenary risers

Rafael Fernandes da Silva [a], Fábio Anderson Fonteles Teófilo [a], Evandro Parente Jr. [a,*], Antônio Macário Cartaxo de Melo [a], Áurea Silva de Holanda [b]

[a] *Laboratório de Mecânica Computacional e Visualização (LMCV), Departamento de Engenharia Estrutural e Construção Civil, Universidade Federal do Ceará, Campus do Pici, Bloco 728, 60440-900 Fortaleza, Ceará, Brazil*

[b] *Departamento de Engenharia de Transportes, Universidade Federal do Ceará, Campus do Pici, Bloco 703, 60440-900 Fortaleza, Ceará, Brazil*

ARTICLE INFO

Article history:
Received 6 July 2011
Received in revised form 12 April 2013
Accepted 13 April 2013

Keywords:
Composite materials
Marine risers
Structural optimization

ABSTRACT

The use of composite risers may offer important advantages over the use of conventional steel risers in deepwater oil fields. However, the design of laminated composite risers is much more complex than the design of steel risers, due to the large number of parameters that need to be chosen to define the riser layup. This work presents a methodology for optimum design of composite catenary risers, where the objective is the minimization of cross-sectional area of the riser and the design variables are the thickness and fiber orientation of each layer of the composite tube. Strength and stability constraints are included in the optimization model and multiple load cases are considered. The methodology can handle both continuous and discrete variables. Gradient-based and genetic algorithms are used in the computer implementation. The proposed methodology is applied to the optimization of composite catenary risers with different water depths, liner materials, and failure criteria. The numerical examples show that the proposed methodology is very robust.

* Corresponding author.
E-mail addresses: rafaeltaua@yahoo.com.br (R.F.da Silva), fabanderson@hotmail.com (F.A.F. Teófilo), evandro@ufc.br (E. Parente), macario@ufc.br (A.M.Cartaxode Melo), aurea@det.ufc.br (Á.S.de Holanda).

0951-8339/$ – see front matter © 2013 Elsevier Ltd. All rights reserved.
http://dx.doi.org/10.1016/j.marstruc.2013.04.002

1. Introduction

The depletion of existing reserves and the increasing demand for oil and gas have led to the search for deepwater fields and research in new technologies to make the production feasible. Fiber reinforced composite materials present several advantages for offshore applications, such as high specific strength and stiffness, high corrosion resistance, low thermal conductivity, excellent damping properties, and high fatigue resistance.

These favorable properties have motivated the oil industry to use composite materials in different offshore applications [30], including risers [22,29,32,34] and stress joints [21]. The reduced weight obtained by the use of composite risers in replacement to steel risers can be substantial, leading to a significant reduction of top tension requirements, which allows the use of simpler and smaller tension mechanisms and smaller platforms [22,30,34].

This work addresses the use of Composite Catenary Risers (CCR) as an alternative to Steel Catenary Risers (SCR) for deepwater fields. The design of laminate composite structures involves a large number of parameters, including the number of layers and the material, thickness, and fiber orientation of each layer. Thus, the use of the conventional trial-and-error strategy is not adequate and optimization techniques have been widely used in the design of laminated composite structures [15].

The use of optimization techniques in the design of marine risers is recent, but the number of applications has been steadily growing. Different optimization algorithms as Sequential Quadratic Programming (SQP) [18], Simulating Annealing (SA) [35], Artificial Immune Systems (AIS) [37], and Particle Swarm Optimization (PSO) [25] have been used for SCR design. Genetic Algorithms (GA) have also been used in the design of SCRs in free hanging and lazy wave configurations [19,35,37,40], since they are very robust, easily deal with discrete variables, non-continuous and non-differentiable functions, and avoid getting trapped by local minima.

This work presents a methodology for optimum design of Composite Catenary Risers in free hanging configuration. The design variables are the thickness and fiber orientation of each layer. The objective is to minimize the cross-sectional area of the riser joint, considering strength and stability constraints. It is important to note that to the best of the authors' knowledge this is the first work dealing with optimization of composite catenary risers.

This paper is organized as follows. Section 2 presents the main components of composite riser joints and discusses the design of composite risers. Section 3 addresses the structural analysis of composite catenary risers and Section 4 describes the optimization model, including the design variables, objective function, and constraints. Section 5 presents the numerical examples. Finally, Section 6 presents the main conclusions.

2. Composite catenary risers

Composite risers are assembled using a series of joints connected to each other by appropriate connections. Riser joints can have short lengths (10–25 m), intermediate lengths (100–300 m), or long lengths (>300 m) [24]. Top tensioned composite risers for drilling and production generally use short joints, but intermediate and long joints may be better suited for catenary risers. There is also potential for the development of spoolable composite risers without intermediate joints, simplifying the transportation and installation [28]. Composite riser joints are composed generally by three elements: liner, composite tube, and terminations [2,23].

The liners are responsible for fluid containment, ensuring the tightness of the riser and avoiding leaking and loss of pressure. These elements are necessary since composite materials are porous and may have micro-cracks. Most composite joints have an inner and an outer liner. Inner liners can be elastomeric, thermoplastic or metallic. In the selection of the inner liner material, in addition to fluid tightness, other aspects should be observed, as cost, adhesiveness to composite and metallic termination, abrasion and corrosion resistance to the reservoir fluid, and impact resistance to mechanical tools inside drilling risers [2,23,34]. The inner liner can also be used as a mandrel during the composite tube manufacturing. The outer liner is constituted generally of synthetic rubber or thermoplastics. In addition to sea-water containment, the outer liner is responsible for protection against external impact and gouging [17,23]. An additional external layer may be used as a mechanical protection from impacts during transportation and handling.

The composite tube is the main structural element of the riser joint. It is constituted by various layers of fibrous composite materials. Carbon and glass fibers are the most used in composite risers, while the matrix is usually a polymeric resin (thermoset or thermoplastic). The material, thickness, and fiber orientation of each layer should be chosen in order to provide sufficient strength and stiffness to the riser joint. A scheme of the riser wall is depicted in Fig. 1.

The joint terminations are metallic pieces composed of two parts: the metal-to-composite interface (MCI) and the connections. The MCI transmits the stresses from the composite tube to the metallic connectors, while the connections are responsible to join the composite joints, assembling the riser. The design of terminations (MCI/connections) is not addressed here, since the major concern of this work is the design of the composite tube.

3. Global–local analysis

Composite structures are generally analyzed by the finite element method (FEM) using solid or shell elements, since these elements allow the consideration of the material, thickness, and orientation of each ply. The use of shell or solid elements yields the stresses and strains in each ply, which are used to verify the design safety using an appropriate failure criterion. However, the modeling of risers using solid or shell elements leads to a prohibitively high computational cost for practical applications. Thus, the analysis of composite risers is carried-out in two levels: global and local. This approach is generally used for flexible risers [39] and has also been recommended for composite risers [12,17,23].

In this approach, the global analysis of the riser is generally carried-out using beam elements, allowing the consideration of dynamic and nonlinear effects due to external loads, floater offset, currents, and waves. The global analysis yields the displacements and stress resultants (axial force, bending and torsional moments) along the riser. However, the use of beam elements does not allow the direct computation of stresses and strains at each ply of the composite tube. Therefore, the stress resultants calculated in global analysis at critical joints are used as input data for local analysis. The local analysis should be carried-out using analytical expressions or finite element (shell or solid) models, since these elements allow the computation of stresses and strains at each ply, as required by the failure criteria of composite materials.

3.1. Global analysis

Since the main objectives are to study the influence of the riser parameters over the optimum design and to assess the robustness and efficiency of the optimization procedure, in the current work the global analysis is performed using an analytical catenary solver, which is much faster than the FEM and provides representative results. Simplified analyses methods have also been used in other formulations for optimum riser design, as catenary solvers [25,37], static finite element analysis [1,18,19], and linearized frequency-domain analysis [35].

The riser axial forces are estimated considering the riser as an inextensible cable subjected to a vertical load distributed along its length [33]. The dry weight of the riser per unit length (w_{dry}) is given

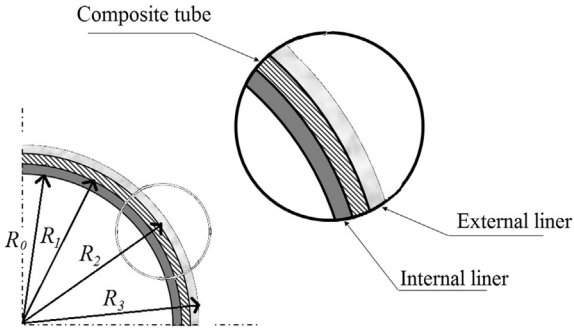

Fig. 1. Composite riser wall.

by the sum of the weight per unit length of the terminations (w_{end}), the internal and external liners (w_{il} and w_{el}), and the composite tube (w_c):

$$\begin{aligned} w_{dry} &= \delta_{end} w_{end} + (1-\delta_{end})(w_c + w_{il} + w_{el}) \\ w_{end} &= \gamma_{end}\pi\left[(R_0 + h_{end})^2 - R_0^2\right], \quad w_c = \gamma_c \pi\left[R_2^2 - R_1^2\right] \\ w_{il} &= \gamma_{il}\pi\left[R_1^2 - R_0^2\right], \quad w_{el} = \gamma_{el}\pi\left[R_3^2 - R_2^2\right] \end{aligned} \tag{1}$$

where δ_{end} is the ratio between the length of terminations and the length of the joint and γ_{end}, γ_c, γ_{il}, and γ_{el}, are the specific weight of the materials employed in the terminations, composite tube, internal and external liner, respectively. The radiuses of each concentric tube (inner liner, composite tube and external liner) are depicted in Fig. 1.

The weight of the internal fluid per unit length (w_{fl}) is added to the dry weight, while the weight of the displaced water per unit length (w_{buo}) is subtracted to provide the effective or apparent weight (w_{ef}) of the riser per unit length:

$$\begin{aligned} w_{ef} &= w_{dry} + w_{fl} - w_{buo} \\ w_{fl} &= \gamma_{fl}\pi R_0^2, \quad w_{buo} = \gamma_{wat}\pi R_3^2 \end{aligned} \tag{2}$$

where γ_{fl} and γ_{wat} are the specific weight of the internal fluid and sea water.

The riser geometry and effective axial force (N_{ef}) are computed by the catenary solver from the effective weight (w_{ef}), top angle with the vertical (α), and sea depth for the mean configuration. At near and far configurations the floater offset (Δ) is applied to the mean configuration, as depicted in Fig. 2.

3.2. Local analysis

In the present work, the classical lamination theory (CLT) is used to perform the local analysis of critical sections of the riser. The internal liner and the composite tube are considered to be perfectly bonded and are analyzed as a single structural system. The external liner is neglected in the local analysis.

The model used in the local analysis is shown in Fig. 3 and consists of a cylindrical structure composed of N layers. The first layer represents the internal metallic liner and the remainder N_c layers constitute the composite tube. The structure is subjected to axial force N_{ef} (obtained from the global analysis), internal pressure p_i and external pressure p_e. The thickness of the kth layer is denoted by h_k.

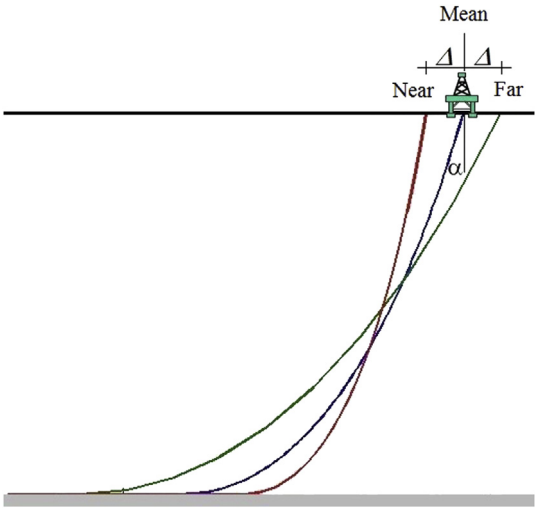

Fig. 2. Catenary riser.

The structure is referenced in a global coordinate system (x, y, z) with origin at the shell middle surface where x is the longitudinal, y is the circumferential, and z is the radial direction. The fiber orientation of the kth layer (θ_k) defines a local coordinate system (x_1, x_2, x_3) where x_1 is parallel to the fibers, x_2 is perpendicular to the fibers, and x_3 is perpendicular to the lamina. The in-plane (membrane) forces in the riser wall are calculated using the theory of thin-walled tubes:

$$\begin{aligned} N_x &= \frac{N_{\text{tw}}}{2\pi R} = \frac{\gamma_{\text{F}}\left(\beta N_{\text{ef}} + p_{\text{i}}\pi R_0^2 - p_{\text{e}}\pi R_2^2\right)}{2\pi R} \\ N_y &= \gamma_{\text{F}}(p_{\text{i}}R_0 - p_{\text{e}}R_2) \\ N_{xy} &= 0 \end{aligned} \tag{3}$$

In this expression, N_{tw} is the true wall force [33], R is the mean radius of the structural system formed by internal liner and composite tube, β is an amplification factor used to account for the environment loads as well as bending, torsion and dynamic effects, and γ_{F} is the load factor used to compute the design forces [11,12]. It is important to note that $N_{xy} = 0$, since torsion is not considered by the catenary solver.

Using the CLT [10,16,27], the generalized stress–strain relationship to laminated composites can be written as:

$$\begin{Bmatrix} \mathbf{N} \\ \mathbf{M} \end{Bmatrix} = \begin{bmatrix} \mathbf{A} & \mathbf{B} \\ \mathbf{B} & \mathbf{D} \end{bmatrix} \begin{Bmatrix} \boldsymbol{\varepsilon}_m \\ \boldsymbol{\kappa} \end{Bmatrix} \tag{4}$$

where $\mathbf{A}$ is the membrane (or extension) stiffness matrix, $\mathbf{D}$ is the bending stiffness matrix, and $\mathbf{B}$ is the bending-extension coupling stiffness matrix, $\boldsymbol{\varepsilon}_m$ is the vector of membrane strains, and $\boldsymbol{\kappa}$ is the vector of curvatures of the laminate. The resultant forces and moments are symbolized by $\mathbf{N} = \{N_x\ N_y\ N_{xy}\}^{\text{t}}$ and $\mathbf{M} = \{M_x\ M_y\ M_{xy}\}^{\text{t}}$, respectively.

In the present work, the riser is subjected only to axisymmetric loads ($\mathbf{M} = \mathbf{0}$). Furthermore, there is no extension-bending coupling ($\mathbf{B} = \mathbf{0}$) due to the axisymmetric characteristic of the riser cross-section. Thus, the stresses at the kth layer in the material coordinate system $\boldsymbol{\sigma}_1^k = \{\sigma_1^k\ \sigma_2^k\ \sigma_{12}^k\}^{\text{t}}$ are computed from:

$$\boldsymbol{\sigma}_1^k = \mathbf{Q}^k\mathbf{T}^k\mathbf{A}^{-1}\mathbf{N} \tag{5}$$

where $\mathbf{Q}^k$ is known as the reduced stiffness matrix [16]and $\mathbf{T}^k$ is the transformation matrix computed from the director cosines of the local axes with respect to the global axes [9].

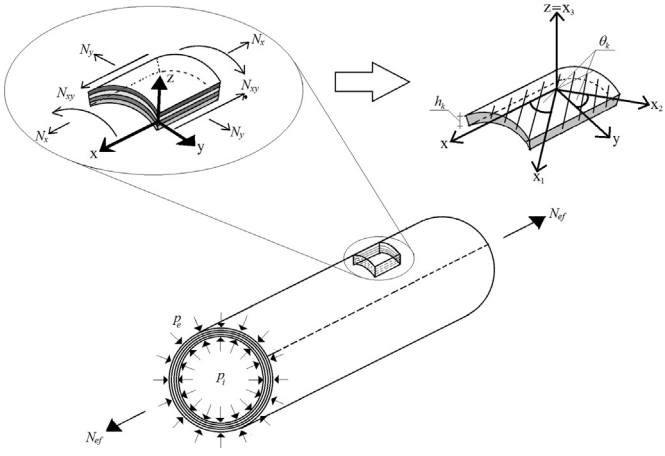

Fig. 3. Composite tube, laminate and material coordinate systems.

3.3. Failure criteria

In the present work, the von Mises failure criterion is employed to verify the strength of the metallic liner, while the strength of the composite layers are checked using the maximum stress or Tsai-Wu failure criteria. The safety factor of the internal liner (SF_{il}) is computed as

$$\begin{aligned} SF_{il} &= \frac{f_y}{\sigma_{vm}} \\ \sigma_{vm} &= \sqrt{\left(\sigma_x^{il}\right)^2 - \sigma_x^{il}\sigma_y^{il} + \left(\sigma_y^{il}\right)^2 + 3\left(\sigma_{yx}^{il}\right)^2} \end{aligned} \tag{6}$$

where f_y is the yielding stress of the metallic material employed in the liner, σ_{vm} is the von Mises stress, and σ_x^{il}, σ_y^{il} and σ_{xy}^{il} are the stresses in the liner, referenced at the global coordinate system.

Using the maximum stress criterion, the safety factor of the kth composite layer (SF_k) is given by

$$\begin{aligned} SF_k &= MIN\left(SF_k^X,\ SF_k^Y,\ SF_k^S\right) \\ SF_k^X &= \begin{cases} \dfrac{X_t}{|\sigma_1^k|}, & \text{if } \sigma_1^k \geq 0 \\ \dfrac{X_c}{|\sigma_1^k|}, & \text{if } \sigma_1^k \leq 0 \end{cases} \\ SF_k^Y &= \begin{cases} \dfrac{Y_t}{|\sigma_2^k|}, & \text{if } \sigma_2^k \geq 0 \\ \dfrac{Y_c}{|\sigma_2^k|}, & \text{if } \sigma_2^k \leq 0 \end{cases} \\ SF_k^S &= \frac{S_{12}}{|\sigma_{12}^k|} \end{aligned} \tag{7}$$

where X_t, X_c, Y_t and Y_c are the tensile and compressive strength of the material parallel and perpendicular to the fiber orientation, while S_{12} is the in-plane shear strength of the material.

Alternatively, the safety factor of the kth layer of the composite tube (SF_k) can be computed using the Tsai-Wu criterion:

$$SF_k = \frac{-b + \sqrt{b^2 + 4a}}{2a} \tag{8}$$

where

$$\begin{aligned} a &= F_{11}\left(\sigma_1^k\right)^2 + F_{22}\left(\sigma_2^k\right)^2 + 2F_{12}\sigma_1^k\sigma_2^k + F_{66}\left(\sigma_{12}^k\right)^2 \\ b &= F_1\sigma_1^k + F_2\sigma_2^k \\ F_1 &= \frac{1}{X_t} - \frac{1}{X_c},\ F_2 = \frac{1}{Y_t} - \frac{1}{Y_c},\ F_{11} = \frac{1}{X_t X_c} \\ F_{22} &= \frac{1}{Y_t Y_c},\ F_{12} = -\frac{1}{2}\sqrt{F_{11}F_{22}},\ F_{66} = \frac{1}{S_{12}^2} \end{aligned} \tag{9}$$

The safety factor of the composite tube can be computed using the first-ply failure (FPF) approach, which states that the laminate fails when a single layer fails. In this case, the safety factor of the composite (SF_c) corresponds to the minimum safety factor of all layers:

$$SF_c = MIN_{k=1}^{Nc}(SF_k) \tag{10}$$

The matrix cracking can be an accepted failure mode in composite risers, since the liners ensure fluid tightness. Thus, a more complex approach based on a progressive failure analysis could be used to evaluate the riser safety factor [12]. However, in order to obtain a conservative design with a small computational cost, the simpler FPF approach was adopted in this work.

3.4. Stability

Thin-walled structures subjected to compressive stresses may collapse due to loss of stability at load levels well below the material strength. Hoop buckling is the local buckling of the tube wall (shell buckling) caused by the compressive stresses generated by external pressure. Hoop buckling is a major concern for deepwater risers and pipelines due to the high hydrostatic pressure, especially when the riser is empty and there is no internal pressure.

The critical pressure of long orthotropic cylindrical shells [12,38] can be computed from:

$$p_{cr} = \frac{3}{R^3}\left(D_{22} - \frac{B_{22}^2}{A_{22}}\right) \tag{11}$$

where A_{22}, B_{22}, and D_{22} are elements of the **A**, **B**, and **D** matrices, Eq. (4), in the hoop direction. It should be noted that $B_{22} = 0$ for symmetric laminates. Finite element analyses of perfect and imperfect cylindrical shells with different lengths and composite layups subjected to external pressure showed that Eq. (11) yields good results for long shells, such as composite riser joints [36]. Furthermore, the buckling pressure of short cylinders is higher than the values given by Eq. (11).

It is well known that unavoidable geometric imperfections reduce the load carrying capacity of compressed shells due to the geometric nonlinear effects. Therefore, the collapse pressure (p_{col}) is obtained by the following expression:

$$p_{col} = k_p p_{cr} \tag{12}$$

where k_p is a reduction factor to account for the effects of the geometric imperfections. A knockdown factor $k_p = 0.75$ is recommended for design purposes [12,38].

The safety factor for hoop buckling is computed by comparing the collapse pressure p_{col} with the differential pressure ($p_e - p_i$) acting on the riser wall. In order to obtain a conservative design, the riser is considered to be empty ($p_i = 0$) and the contribution of the internal liner to the buckling pressure (p_{cr}) is neglected. Thus, the safety factor for buckling is computed from:

$$SF_{bck} = \frac{p_{col}}{\gamma_F p_e} \tag{13}$$

4. Optimization model

This section presents the proposed optimization model for laminated composite risers. The input data of the problem includes the loads, material properties, number of layers (N_c) of the composite tube, inner radius (R_0), thickness of internal and external liners (h_{il}, h_{el}), amplification factor (β), force coefficient (γ_F), and required safety factors. The objective is to find the best (i.e. lowest cost) laminate that meets the strength and stability requirements of the composite riser.

4.1. Design variables

The thicknesses (h_k) and the fiber orientation angles (θ_k) of each ply of the composite tube (Fig. 4) are adopted as design variables. Since only symmetric layups are allowed, the design variables are

$$x = \{ h_1 \quad h_2 \quad \ldots \quad h_{N_c/2}\ \theta_1 \quad \theta_2 \quad \ldots \quad \theta_{N_c/2} \}^{\mathrm{t}} \tag{14}$$

The riser weight is unaffected by the fiber orientations of each layer and is function of both thickness and material of each layer. The same occurs with the catenary geometry and forces, since they depend on the riser weight.

The layup is constant along the riser, since considering different properties along the riser length would increase the design space and the computational cost. Furthermore, the use of riser joints with different layups could increase the manufacture costs.

Most works dealing with optimization of laminated structures consider that design variables can only assume discrete values [13,26], but continuous variables have also been used [7]. Since the choice between continuous and discrete variables is driven mainly by manufacturing issues, both options are considered here, originating two models: *continuous* and *discrete*. In the *continuous model*, the design variables are limited by lower and upper bounds:

$$\left.\begin{array}{l} \theta_{\min} \le \theta_k \le \theta_{\max} \\ h_{\min} \le h_k \le h_{\max} \end{array}\right\} k = 1, \ldots, \frac{N_c}{2} \tag{15}$$

On the other hand, the design variables of the *discrete model* can only assume a set of predefined values ($\boldsymbol{\theta}_{\mathrm{p}}$ and $\mathbf{h}_{\mathrm{p}}$):

$$\begin{array}{l} \boldsymbol{\theta}_{\mathrm{p}} = \{\theta_{\min}, \theta_{\min} + \Delta\theta, \theta_{\min} + 2\Delta\theta, \ldots, \theta_{\max}\}^{\mathrm{t}} \\ h_{\mathrm{p}} = \{h_{\min}, h_{\min} + \Delta h, h_{\min} + 2\Delta h, \ldots, h_{\max}\}^{\mathrm{t}} \end{array} \tag{16}$$

where $\Delta\theta$ and Δh are user supplied increments.

4.2. Objective function

Different objective functions have been used in the optimization of composite structures. In minimization problems, weight, deflection, and cost of composite panels [5], thickness of composite plates [4], and the sensitivity of buckling loads due to variations in ply angles[3] have been used as objective functions. Maximization of natural frequencies and buckling loads has also been considered [1].

In the present work, the cost of the riser joint is considered proportional to the volume of composite material. Thus, the objective is to minimize the cross-sectional area of the composite tube. In order to

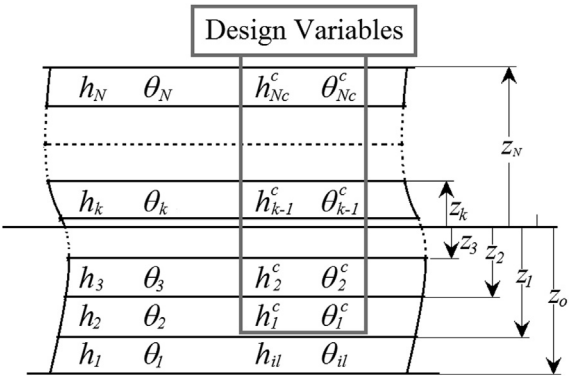

Fig. 4. Composite layup.

improve the convergence of the optimization algorithm, a normalized cross-sectional area of the composite tube is used as objective function $f(\mathbf{x})$:

$$f(\mathbf{x}) = \frac{A(\mathbf{x}) - A_{\min}}{A_{\max} - A_{\min}} \tag{17}$$

where $A(\mathbf{x})$, $A_{\min}$ and $A_{\max}$ are the current, minimum and maximum cross-sectional area of the composite tube, respectively. The minimum area is obtained considering all layers of the composite tube with $h_k = h_{\min}$ and the maximum with $h_k = h_{\max}$.

4.3. Constraints

Strength and stability constraints are considered in order to ensure the structural integrity of the riser. Based on previous catenary riser analyses, two critical load cases were chosen. Load Case A corresponds to the riser filled with internal fluid at far configuration, leading to high tension at the top riser joint. On the other hand, Load Case B corresponds to the riser without internal fluid at the near configuration, leading to high external pressure and true wall compression in the touchdown point (TDP) of the riser. In this case, a conservative design is adopted in which the small effective force at TDP and the internal pressure are neglected ($N_{\text{ef}}^{\text{bot}} = 0$, $p_i = 0$) in the local analysis.

In Load Case A, the local analysis is executed applying the effective top tension ($N_{\text{ef}}^{\text{top}}$) obtained in the global analysis and the internal pressure of the fluid (p_{i}). The stresses computed from the local analysis are used to calculate the internal liner safety factor ($\text{SF}_{\text{il}}^{\text{top}}$) and the composite safety factor ($\text{SF}_{\text{c}}^{\text{top}}$) at the top end. Thus, the constraints related to the liner and composite safety factors are defined as:

$$\begin{aligned} g_{\text{il}}^{\text{top}} &= 1 - \frac{\text{SF}_{\text{il}}^{\text{top}}}{\text{SF}_{\text{il}}^{\text{req}}} \leq 0 \\ g_{\text{c}}^{\text{top}} &= 1 - \frac{\text{SF}_{\text{c}}^{\text{top}}}{\text{SF}_{\text{il}}^{\text{req}}} \leq 0 \end{aligned} \tag{18}$$

where $\text{SF}_{\text{il}}^{\text{req}}$ and $\text{SF}_{\text{c}}^{\text{req}}$ are the required safety factor of the liner and the composite, respectively.

In the Load Case B, the stresses computed from the local analysis with the riser subjected only to external pressure allow the calculation of the liner and composite safety factor and the buckling safety factor at the bottom of the riser ($\text{SF}_{\text{il}}^{\text{bot}}, \text{SF}_{\text{c}}^{\text{bot}}, \text{SF}_{\text{bck}}$) corresponding to the TDP joint. The constraints related to the liner and composite safety factors are defined as:

$$\begin{aligned} g_{\text{il}}^{\text{bot}} &= 1 - \frac{\text{SF}_{\text{il}}^{\text{bot}}}{\text{SF}_{\text{il}}^{\text{req}}} \leq 0 \\ g_{\text{c}}^{\text{bot}} &= 1 - \frac{\text{SF}_{\text{c}}^{\text{bot}}}{\text{SF}_{\text{c}}^{\text{req}}} \leq 0 \end{aligned} \tag{19}$$

The stability constraint is implemented in the normalized form:

$$g_{\text{bck}} = 1 - \frac{\text{SF}_{\text{bck}}}{\text{SF}_{\text{bck}}^{\text{req}}} \leq 0 \tag{20}$$

where $\text{SF}_{\text{bck}}^{\text{req}}$ is the required Safety Factor to avoid hoop buckling as defined in Section 3.4.

Finally, the complete optimization model for composite catenary risers is given by:

$$\text{Find} \quad x = \left\{ h_1 \quad h_2 \quad \ldots \quad h_{N_c/2}\, \theta_1 \quad \theta_2 \quad \ldots \quad \theta_{N_c/2} \right\}^{\mathrm{t}}$$

$$\text{That minimizes} \quad f(x) = \frac{A(x) - A_{\min}}{A_{\max} - A_{\min}}$$

Subjected to :

$$\begin{aligned}
g_{\mathrm{il}}^{\mathrm{top}} &= 1 - \frac{\mathrm{SF}_{\mathrm{il}}^{\mathrm{top}}}{\mathrm{SF}_{\mathrm{il}}^{\mathrm{req}}} \leq 0 \\
g_{\mathrm{c}}^{\mathrm{top}} &= 1 - \frac{\mathrm{SF}_{\mathrm{c}}^{\mathrm{top}}}{\mathrm{SF}_{\mathrm{c}}^{\mathrm{req}}} \leq 0 \\
g_{\mathrm{il}}^{\mathrm{bot}} &= 1 - \frac{\mathrm{SF}_{\mathrm{il}}^{\mathrm{bot}}}{\mathrm{SF}_{\mathrm{il}}^{\mathrm{req}}} \leq 0 \\
g_{\mathrm{c}}^{\mathrm{bot}} &= 1 - \frac{\mathrm{SF}_{\mathrm{c}}^{\mathrm{bot}}}{\mathrm{SF}_{\mathrm{c}}^{\mathrm{req}}} \leq 0 \\
g_{\mathrm{bck}} &= 1 - \frac{\mathrm{SF}_{\mathrm{bck}}}{\mathrm{SF}_{\mathrm{bck}}^{\mathrm{req}}} \leq 0
\end{aligned} \tag{21}$$

If design variables have continuous values :

$$\theta_{\min} \leq \theta_k \leq \theta_{\max}$$

$$h_{\min} \leq h_k \leq h_{\max}$$

If design va riables have discrete values :

$$\theta_k \in \{\theta_{\min}, \theta_{\min} + \Delta\theta, \theta_{\min} + 2\Delta\theta, \ldots, \theta_{\max}\}$$

$$h_k \in \{h_{\min}, h_{\min} + \Delta h, h_{\min} + 2\Delta h, \ldots, h_{\max}\}$$

Fatigue caused by environmental conditions and vortex induced vibrations (VIV) is an important issue in the design of catenary risers. However, evaluation of fatigue life requires the use of complex and costly finite element analysis in time or frequency domains. These procedures were not included in the model to keep the computational cost low, in order to allow the use of the model in personal computers. As a consequence, the solution of this optimization problem should be seen as preliminary designs to be used as input for more advanced analysis procedures.

4.4. Computer implementation

The optimization model described previously was implemented in MATLAB and three different optimization methods can be used to find a solution. The first method uses the gradient-based sequential quadratic programming (SQP) algorithm via the *fmincon* routine of the MATLAB Optimization Toolbox [20]. This method can be applied to nonlinear constrained problems with continuous variables.

The second method uses the penalty function (PF) approach presented by [31] to solve discrete optimization problems using gradient-based methods. In this approach, the problem is initially solved considering that design variables are continuous. After that, the variables with non-discrete values are penalized replacing the original objective function $f(\mathbf{x})$ by the modified objective function $F(\mathbf{x})$:

$$F(\mathbf{x}) = f(\mathbf{x}) + s \sum_{i=1}^{N_{\mathrm{d}}} \phi_{\mathrm{d}}^{i}(\mathbf{x}) \tag{22}$$

where s is the penalty parameter, N_{d} is the number of discrete variables, and $\phi_{\mathrm{d}}^{i}(x_i)$ is the penalty function for non-discrete values of the ith discrete design variable, which is given by

$$\phi_{\mathrm{d}}^{i}(x_i) = \frac{1}{2}\left(\sin\frac{2\pi\left[x_i - 0.25\left(d_{ij+1} + 3d_{ij}\right)\right]}{d_{ij+1} - d_{ij}} + 1\right) \tag{23}$$

where d_{ij} is the jth discrete value that the ith design variable can assume. The problem should be solved repeatedly for increasing values of the penalty parameter [31]. This strategy was combined with the gradient-based SQP algorithm. The gradients were evaluated using finite differences.

One of the main drawbacks of gradient-based optimization methods is their susceptibility to be attracted by local minima. To overcome this problem, the Multistart method [6] was adopted for both continuous and discrete problems. In this procedure, N_{run} initial designs satisfying the bound constraints in θ_k and h_k are randomly generated and used as starting points for N_{run} independent optimizations. In the computer implementation, the optimizations are carried-out sequentially and if the new solution has a smaller objective function value than the current best design, then the best design is updated. If a sufficiently high number of different starting points are used, then the best design will be close to the global optimum.

The third solution method is a genetic algorithm (GA) implemented using well-known GA libraries [8] and integer encoding. Genetic algorithms apply concepts of genetics combined with Darwin's theory of evolution [14] and can be used to obtain optimum solutions of continuous and discrete problems. Since GAs are zero-order methods, they do not require the computation of the gradients of objective and constraint functions. Furthermore, the use of a set (population) of designs and the random character of GA operators (e.g. selection, crossover, and mutation) help the method to avoid being trapped by local minima and find the global minimum. On the other hand, the GA is more time consuming than the SQP method. The implemented GA for discrete problems is described below.

First, an initial population is randomly generated containing N_{ind} individuals or candidate solutions. Each individual is represented by an integer array (chromosome) of the design variables and has its objective function and constraints evaluated. In order to consider constraints violation, a static penalty method is used and the penalized objective function is obtained for each design, according to:

$$F(\mathbf{x}) = f(\mathbf{x}) + k_{\mathrm{p}} \sum_{i=1}^{N_g} \max(g_i(x), 0) \tag{24}$$

where k_{p} is the penalty factor and g_i is the ith constraint. Then, the individuals are sorted in decreasing order of their penalized objective function and a fitness score based on the rank position is assigned to each individual. Individuals with the smaller penalized objective functions have greater fitness scores and more chances to survive and transmit their characteristics to next generation (iteration).

The stochastic uniform selection [8] is applied on the whole population and a group of $N_{\mathrm{sel}} = C_{\mathrm{r}} N_{\mathrm{ind}}$ individuals (parents), where C_{r} is known as crossover rate, is selected to perform the crossover. Crossover is a key genetic operator for GA convergence. This operator is sequentially applied to pairs of parents and produces two new individuals, called sons, which combine traits of both parents.

The mask crossover, depicted in Fig. 5, is employed in this work. The mask is obtained by randomly generating a number (1 or 2) for each variable. If the mask value is 1, the son A inherits the design variable from parent A. Otherwise, the value comes from parent B. The opposite is applied to son B. Since two sons are created from two parents, the total number of sons is equal to the number of parents.

Even though GAs have lower probability to be trapped in local minima than gradient-based methods, premature convergence to local minima can occur. To prevent it, genetic variability has to be maintained. The mutation operator is one of the strategies used to ensure variability within the population, and it is applied in the sons generated by the crossover process. It has a low probability of occurring, symbolized by P_{m}. For each gene of the chromosome, a random number between 0 and 1 is generated. If such number is smaller than P_{m}, a random integer satisfying Eq. (16) replaces the original gene value (Fig. 6).

Finally, a new population is formed by replacing the lesser fit parents with the sons. In this way, the best $1 - C_{\mathrm{r}}$ individuals of the old population are preserved (elitism selection). The process is repeated until a certain number of generations are reached (N_{gen}).

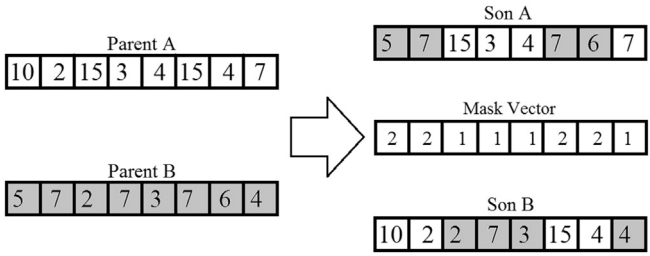

Fig. 5. Crossover operator.

5. Numerical examples

This section presents numerical examples in order to study the behavior of the optimization model presented in Section 4. The optimum designs are achieved considering continuous and discrete design variables. The continuous problem is solved using the SQP method, while the discrete problem is solved by both PF and GA approaches described in Section 4.4. The crossover rate (C_r) and mutation probability (P_m) of the GA are set at 0.90 and 0.05, respectively. Data related to all examples are showed in Tables 1 and 2.

5.1. Example 1

In this first example, the sea depth is considered as 2500 m, the top angle is 20°, and the yield stress of the steel liner is $f_y = 448.2$ MPa (API X65). The problem is firstly solved adopting the Tsai-Wu failure criterion for the composite layers. The optimum designs obtained are presented in Table 3. Only one global optimum solution was found for the continuous problem. The active constraints are related to the material failure of the composite in Load Case A and the buckling constraint in Load Case B. It is important to note that this problem has multiple optimal solutions with the same cost.

The behavior of the objective function and the maximum constraint violation in the optimization process are shown for SQP solution in Fig. 7 and for GA solution in Fig 8. From Fig. 7 it can be noted that the starting point is an unfeasible design. Initially the objective function increases while the maximum constraint violation decreases to near zero values. Then, the objective function starts to decrease.

The riser effective weight per unit length (w_{ef}) and the forces on the top of the riser are presented in Table 4 for the optimum discrete solutions. The forces and weights corresponding to the continuous solutions are not presented, since they are very close to the discrete solution.

The behavior of the GA depends on the chosen parameters. The reliability (R) is the ratio of number of successful runs (N_{opt}) to the total number of optimizations (N_{run}). The effect of population size (N_{ind}) and number of generations (N_{gen}) on the GA reliability is showed in Table 5. Clearly, the effect of the increment on population size is more significant than the number of generations. Maximum reliability is almost obtained with $N_{ind} = 200$ and $N_{gen} = 50$ ($R = 0.96$) whereas only 76% of reliability is reached with $N_{ind} = 50$ and $N_{gen} = 200$, both with the same number of objective function evaluations. Fig. 8 depicts GA run for a population size of 100, which shows that an optimum design can be reached with fewer generations.

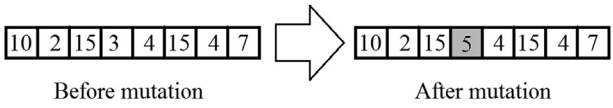

Fig. 6. Mutation operator.

Table 1
Numerical data used in the examples.

Design parameters	Internal radius [R_i] (m)	0.125
	Number of layers of the composite tube [N_c]	10
	Thickness of the inner (steel) liner [h_{il}] (m)	0.006
	Internal pressure [p_i] (MPa)	25.0
	Floater offset [Δ_{os}]	7.5% of water depth
	Amplification factor [β]	1.5
	Force coefficient [γ_F]	1.1
	Thickness of the external liner [h_{el}](m)	0.04
	Specific weight – internal fluid [γ_{if}] (kN/m^3)	7.0
	Specific weight – sea water [γ_{wat}] (kN/m^3)	10.05
	Specific weight –external liner [γ_{el}] (kN/m^3)	9.0
	Fraction of the termination [δ_{end}]	0.15
Continuous variables	Minimum and maximum ply thicknesses (mm)	$1 \le t_k \le 10$
	Minimum and maximum fiber orientation angles	$-90^\circ \le \theta_k \le 90^\circ$
Discrete variables	Allowable ply thicknesses (mm)	{1, 2, …, 9, 10}
	Allowable fiber orientation angles	{0, ±5°, ±10°, …, 90°}
Constraints	Required buckling safety factor [SF_{bck}^{req}]	3.0
	Required metallic inner liner safety factor [SF_{il}^{req}]	1.5
	Required composite tube safety factor [SF_c^{req}]	3.0

The reliability and computational costs for the three optimization methods are compared in Table 6. The computational cost is measured by the average number of objective function evaluations for N_{run} optimizations:

$$N_{fev} = \frac{\sum_{i=1}^{N_{run}} N_{fev}^i}{N_{run}} \tag{25}$$

where N_{fev}^i is the number of objective function evaluations of the ith optimization. The number of function evaluations for the SQP method is different for each optimization, since it depends on the starting point. The number of function evaluations of the GA method is constant:

$$N_{fev} = N_{fev}^i = N_{ind} + N_{ind} C_r N_{gen}, \quad i = 1, 2, \ldots, N_{run} \tag{26}$$

As expected, the SQP has the smallest N_{fev}. The GA gives the greatest computational cost, but has an excellent reliability. Though the PF presents a small computational cost ($N_{fev} = 1857$), its reliability is

Table 2
Material properties [16,27,30].

Composite	E_1 (GPa)	137.0
	E_2 (GPa)	9.0
	G_{12} (GPa)	7.1
	υ_{12}	0.3
	F_{1t} (MPa)	1517
	F_{1c} (MPa)	1034
	F_{2t} (MPa)	34.48
	F_{2c} (MPa)	151.7
	F_6 (MPa)	68.90
	Specific weight (kN/m^3)	15.70
Steel	E (GPa)	210
	υ	0.3
	Specific weight (kN/m^3)	76.52

Table 3
Global optimum solutions for Example 1 – Tsai-Wu.

Model	Design variables h(mm), θ(degree)		Safety factors					h_t (mm)
			Load Case A		Load Case B			
			SF_{il}^{top}	SF_{c}^{top}	SF_{il}^{bot}	SF_{c}^{bot}	SF_{bck}	
Continuous variables (SQP)	h	[6.510/1.000/1.001/1.021/1.112]s	1.519	3.000	1.553	13.48	3.000	21.29
	θ	[90.000/0.000/0.000/0.000/0.000]s						
Discrete variables (PF)	h	[4/1/1/2/3]s	1.594	3.238	1.524	12.77	3.172	22
	θ	[90/90/90/0/0]s						
	h	[5/1/1/1/3]s	1.536	3.037	1.548	13.06	3.205	22
	θ	[90/90/0/−50/0]s						
	h	[5/1/1/1/3]s	1.531	3.0188	1.554	13.26	3.215	22
	θ	[90/90/0/−55/0]s						
	h	[2/4/1/3/1]s	1.535	3.0166	1.563	13.21	3.243	22
	θ	[90/90/−55/5/5]s						
Discrete variables (GA)	h	[1/1/4/1/4]s	1.534	3.021	1.532	12.50	3.027	22
	θ	[80/65/90/65/−5]s						
	h	[3/2/1/3/2]s	1.592	3.233	1.514	12.44	3.119	22
	θ	[90/80/−80/5/−5]s						
	h	[2/4/1/1/3]s	1.58	3.190	1.527	12.80	3.153	22
	θ	[−85/90/15/−5/5]s						
	h	[1/5/2/1/2]s	1.53	3.073	1.519	12.66	3.175	22
	θ	[90/90/15/0/0]s						

small, showing that meta-heuristics algorithms, as GAs, are better suited to discrete optimization problems.

This example was also solved using the maximum stress criterion for the composite layers. The optimum designs are showed in Table 7. It can be noted that the composite tubes are thicker than the solution obtained for Tsai-Wu. In addition, multiple continuous solutions were found, all of them with cross-ply layups. Steel liner failure becomes active in Load Case B and buckling constraint is active only in one solution. The riser thicknesses obtained by Tsai-Wu and maximum stress have close values, but the composite safety factor in Load Case B was reduced almost by the half when the maximum stress was used as failure criterion, showing its conservative character.

It can be observed that there are not strictly active constraints in all optimum designs with discrete variables. However, the safety factors regarding to composite failure in Load Case A are very close to the minimum required values.

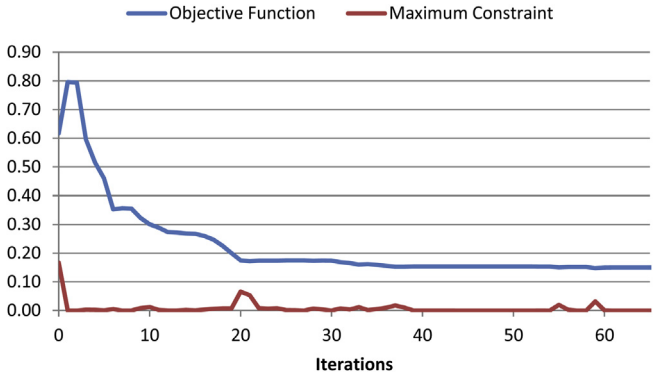

Fig. 7. Optimization history (SQP).

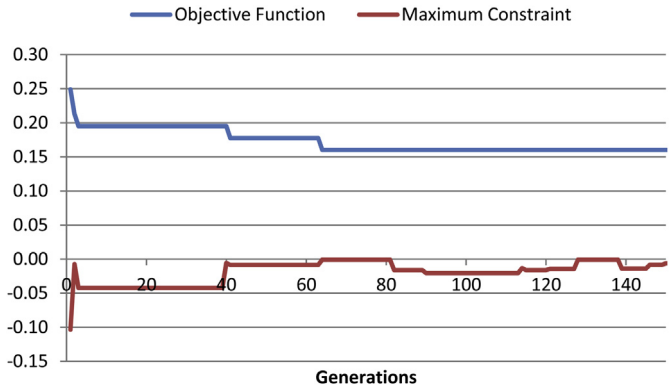

Fig. 8. Optimization history (GA).

Table 4
Optimum riser designs: weight and forces.

Example	Forces on the top of the riser (kN)			w_{ef} (kN/m)
	Horizontal	Vertical	Tension	
1. Tsai-Wu	550.63	1105.64	1235.17	0.2738
1. Max. stress	561.01	1126.49	1258.46	0.2790
2	725.06	1455.88	1626.44	0.3005
3	805.62	1268.93	1503.06	0.2790
4	550.63	1105.64	1235.17	0.2738

5.2. Example 2

This example uses the same data of Example 1 (Section 5.1) with the Tsai-Wu criterion for the laminate, but the sea depth was increased to 3000 m. From now on, $N_{run} = 50$ for all optimization methods and $N_{ind} = N_{gen} = 150$ for the GA. The obtained results are presented in Table 8. There are

Table 5
GA reliability dependence on N_{ind} and N_{gen} ($N_{run} = 50$).

N_{ind}	N_{gen}			
	50	100	150	200
50	0.28	0.48	0.58	0.76
100	0.70	0.86	0.96	1.00
150	0.82	0.98	1.00	1.00
200	0.96	1.00	0.98	1.00

Table 6
Comparison between optimization methods ($N_{run} = 50$).

Parameter	Models				
	SQP (cont.)	PF (disc.)	GA ($N_{ind} \times N_{gen}$)		
			50 × 50	100 × 100	150 × 150
R	0.6	0.08	0.28	0.86	1.00
N_{fev}	1438	1857.5	2300	9100	20,400

Table 7
Global optimum solutions for Example 1 – maximum stress.

Model	Design variables h(mm), θ(degree)		Safety factors					h_t
			Load Case A		Load Case B			
			SF_{il}^{top}	SF_{c}^{top}	SF_{il}^{bot}	SF_{c}^{bot}	SF_{bck}	
Continuous variables (SQP)	h	[3.154/1.812/1.238/1.271/3.958]s	1.651	3.000	1.500	5.684	3.000	22.87
	θ	[90.00/0.000/90.00/90.00/0.000]s						
	h	[5.663/1.002/1.003/1.024/2.740]s	1.651	3.000	1.500	5.694	3.404	22.87
	θ	[90.00/0.009/−0.007/0.002/−0.000]s						
Discrete variables (PF)	h	[1/5/1/1/4]s	1.686	3.076	1.530	5.830	3.101	24
	θ	[0/90/0/90/0]s						
	h	[4/2/2/2/2]s	1.69	3.073	1.520	5.785	3.281	24
	θ	[-85/0/0/80/0]s						
	h	[5/2/1/2/2]s	1.687	3.057	1.530	5.830	3.746	24
	θ	[90/0/90/0/0]s						
	h	[1/5/3/1/2]s	1.686	3.057	1.530	5.830	3.903	24
	θ	[90/90/0/0/0]s						
Discrete variables (GA)	h	[1/1/5/4/1]s	1.689	3.065	1.517	5.742	3.009	24
	θ	[5/70/90/−5/0]s						
	h	[4/2/2/2/2]s	1.673	3.002	1.522	5.777	3.172	24
	θ	[80/10/−5/90/−20]s						
	h	[5/3/1/2/1]s	1.673	3.017	1.537	5.864	3.688	24
	θ	[90/5/−85/10/−15]s						
	h	[1/5/1/4/1]s	1.678	3.030	1.514	5.888	3.855	24
	θ	[85/85/15/−5/0]s						

Table 8
Global optimum solutions for Example 2.

Model	Design variables h(mm), θ(degree)		Safety factors					h_t
			Load Case A		Load Case B			
			SF_{il}^{top}	SF_{c}^{top}	SF_{il}^{bot}	SF_{c}^{bot}	SF_{bck}	
Continuous variables (SQP)	h	[1.008/1.000/1.464/3.639/8.585]s	1.587	3.000	1.500	13.55	3.031	31.39
	θ	[0.000/0.000/90.00/0.000/90.00]s						
	h	[2.924/3.643/1.004/7.124/1.000]s	1.587	3.000	1.500	13.55	4.781	31.39
	θ	[90.00/0.000/−0.003/90.00/−0.005]s						
	h	[1.055/7.891/1.013/4.593/1.145]s	1.587	3.000	1.500	13.55	5.947	31.39
	θ	[0.000/90.00/90.00/0.000/90.00]s						
	h	[7.869/1.068/3.476/2.172/1.112]s	1.587	3.000	1.500	13.55	7.069	31.39
	θ	[90.00/90.00/0.000/0.000/90.00]s						
Discrete variables (PF)	h	[1/4/1/1/9]s	1.624	3.084	1.505	13.51	3.186	32
	θ	[90/0/0/0/90]s						
	h	[1/1/10/3/1]s	1.616	3.063	1.506	13.84	5.447	32
	θ	[-10/0/90/5/0]s						
	h	[1/1/8/5/1]s	1.624	3.084	1.505	13.51	6.321	32
	θ	[0/90/90/0/90]s						
	h	[7/2/1/3/3]s	1.624	3.084	1.505	13.51	7.985	32
	θ	[90/0/0/90/0]s						
Discrete variables (GA)	h	[7/1/4/1/3]s	1.596	3.010	1.507	13.53	6.770	32
	θ	[90/25/−5/−5/85]s						
	h	[9/1/1/1/4]s	1.617	3.064	1.504	13.48	7.508	32
	θ	[90/10/−5/75/−5]s						
	h	[9/1/1/4/1]s	1.593	3.001	1.509	13.58	7.567	32
	θ	[90/10/−80/−5/25]s						
	h	[1/7/1/1/6]s	1.602	3.039	1.501	13.45	7.623	32
	θ	[−85/90/90/90/5]s						

multiple global optimum solutions for all approaches. As expected, the risers are thicker than in previous example, due to the increase in axial force in Load Case A (see Table 4) and external pressure in Load Case B.

Comparing solutions in Example 1 and Example 2, there is an increase in the safety factors of the internal liner in Load Case A and of the composite in Load Case B. Once again, for the continuous problem, the active constraints are related to the composite failure in Load Case A and liner failure in Load Case B. Only one design presents active buckling constraint, a continuous one. Continuous and PF solutions have cross-ply layups.

Analyzing the fiber angles of discrete optimum solutions, it is observed that the PF approach reaches many cross-ply layups, similar to continuous solutions, while the use of GA leads to designs with greater diversity.

Though the global optimum designs have similar values for their liner and composite safety factors (SF_{il} and SF_c), their buckling safety factors (SF_{bck}) vary greatly for each optimization algorithm. For the SQP, for example, the buckling safety factors range from 3.031 to 7.069. Intervals of the buckling safety factor to PF and AG are respectively [3.186, 7.985] and [6.77, 7.623]. In these cases, the solution with the highest buckling safety factor could be considered as the best.

5.3. Example 3

This example uses the same data of Example 1 (Section 5.1) with Tsai-Wu criterion, but the top angle was increased to 25°. Some global optimum designs are presented in Table 9. Compared to Example 1, the solutions obtained here present higher values for riser thickness, since the top tension increases with the catenary top angle (see Table 4). The large top tension makes the composite failure constraint active for Load Case A. The liner constraint is active in both load cases for all continuous

Table 9
Global optimum solutions for Example 3.

Model	Design variables h(mm), θ(degree)		Safety factors					h_t (mm)
			Load Case A		Load Case B			
			SF_{il}^{top}	SF_c^{top}	SF_{il}^{bot}	SF_c^{bot}	SF_{bck}	
Continuous variables (SQP)	h	[3.674/1.553/1.000/1.000/3.997]s	1.500	3.001	1.500	12.28	3.000	22.45
	θ	[90.00/−0.101/90.00/90.00/0.053]s						
	h	[3.101/1.0239/2.573/3.491/1.036]s	1.500	3.001	1.500	12.28	3.019	22.45
	θ	[89.99/−0.0.61/90.00/0.010/0.009]s						
	h	[1.573/2.619/1.627/1.482/3.924]s	1.500	3.001	1.500	12.28	3.069	22.45
	θ	[90.00/−89.994/−0.038/89.972/0.010]s						
	h	[1.393/1.838/2.443/3.561/1.989]s	1.500	3.001	1.500	12.28	3.262	22.45
	θ	[−89.72/90.00/89.97/0.130/−0.131]s						
Discrete variables (PF)	h	[4/1/1/5/1]s	1.551	3.116	1.518	12.29	3.502	24
	θ	[90/0/90/0/75]s						
	h	[4/1/1/5/1]s	1.550	3.107	1.530	12.53	3.603	24
	θ	[90/90/0/0/90]s						
	h	[5/2/1/2/2]s	1.550	3.107	1.530	12.53	3.746	24
	θ	[90/0/90/0/0]s						
	h	[1/2/2/1/6]s	1.550	3.107	1.530	12.53	3.904	24
	θ	[90/90/90/90/0]s						
Discrete variables (GA)	h	[1/2/4/1/4]s	1.545	3.105	1.507	11.79	3.009	24
	θ	[15/−75/90/−10/0]s						
	h	[2/1/3/5/1]s	1.524	3.071	1.537	12.46	3.181	24
	θ	[80/20/90/−10/90]s						
	h	[5/1/3/2/1]s	1.532	3.037	1.527	12.29	3.562	24
	θ	[85/−15/10/−10/90]s						
	h	[2/4/1/1/4]s	1.529	3.032	1.538	12.50	3.794	24
	θ	[−80/85/−10/30/−5]s						

Table 10
Global optimum solutions for Example 4.

Model	Design variables h(mm), θ(degree)		Safety factors					h_t (mm)
			Load Case A		Load Case B			
			SF_{il}^{top}	SF_{c}^{top}	SF_{il}^{bot}	SF_{c}^{bot}	SF_{bck}	
Continuous variables (SQP)	h	[6.5102/1.052/1.020 1.023/1.039]s	1.869	3.000	1.911	13.48	3.000	21.29
	θ	[90/−0.025/0.0148/0.006/0.004]s						
Discrete variables (PF)	h	[1/4/1/3/2]s	1.9611	3.238	1.876	12.77	3.172	22
	θ	[90/90/90/0/0]s						
	h	[5/1/1/1/3]s	1.9149	3.088	1.904	13.12	3.190	22
	θ	[90/90/5/−40/5]s						
	h	[4/1/1/1/4]s	1.8836	3.004	1.921	13.36	3.220	22
	θ	[90/90/−60/−80/5]s						
	h	[5/1/1/3/1]s	1.8789	3.003	1.919	13.38	3.229	22
	θ	[90/60/90/0/0]s						
Discrete variables (GA)	h	[5/2/1/1/2]s	1.8948	3.017	1.88	12.50	3.004	22
	θ	[−85/40/−40/15/−15]s						
	h	[2/3/1/2/3]s	1.925	3.110	1.887	12.73	3.090	22
	θ	[−85/80/85/−25/5]s						
	h	[2/3/1/2/3]s	1.9274	3.138	1.884	12.77	3.096	22
	θ	[−80/90/90/20/0]s						
	h	[6/1/1/2/1]s	1.9326	3.162	1.881	12.82	3.176	22
	θ	[90/20/−5/0/10]s						

designs. Again it is noted the tendency for the PF approach to lead to cross-ply layups, which does not occur for the GA approach.

5.4. Example 4

This example uses the same data from Example 1 (Section 5.1) with Tsai-Wu criterion, but the yield stress of the steel liner was increased to $f_y = 551.6$ MPa (API X80). The obtained results are presented in Table 10. In comparison with Example 1 the single continuous solution presents the same layup and the use of high strength steel only increased the liner safety factors, since the solution is governed by composite failure (Load Case A) and buckling (Load Case B) constraints. Multiple solutions with different layups were found by the discrete approaches (PF and GA). It is interesting to note that the use of a high strength steel (API X80) did not lead to a lighter riser, since the optimum design has the same riser thickness obtained in Example 1 (API X65).

6. Conclusion

This paper addressed the use of composite catenary risers as an alternative to deepwater applications and presented a methodology for optimum design of these risers. The results showed that the proposed model and its computer implementation are very robust, since optimum solutions were found for all numerical examples. The SQP for continuous variables is the most efficient, while GA is the most time consuming. However, GA solutions have greater diversity, presenting more choices to the designer.

The riser thicknesses for discrete designs are larger than the thickness obtained for continuous solutions, but the difference is generally small. In fact, most of discrete solutions have a continuous counterpart with slightly small cost. Furthermore, the majority of numerical examples have multiple global solutions, for both continuous and discrete problems, offering different options to the designer. As an example, in most of the problems the stress safety factors of different designs are very close to each other, but the buckling pressure presents large variation. In this case the designer can choose the laminate with the largest buckling pressure.

It was observed that the required composite thickness, and so the riser cost, increases with water depth and top angle. On the other hand, the use of high strength steel for inner liner does not reduce the laminate thickness since the composite tube is designed to be the load bearing element of the composite riser, enabling the use of thermoplastic or elastomeric liners. Finally, the use of Tsai-Wu resulted in less conservative designs than the use of maximum stress criterion.

The optimization model presented here was based on the use of a simple and efficient analysis procedure, where the dynamic effects were considered using an amplification factor that can be chosen to obtain a conservative design. Therefore, the obtained solutions should be seen as preliminary designs since environment loads, bending, torsion, VIV and fatigue are not included. These preliminary designs could be used as input for a more detailed analysis.

Acknowledgments

The financial support by CNPq (Conselho Nacional de Desenvolvimento Científico e Tecnológico), CAPES (Coordenação de Aperfeiçoamento de Pessoal de Nível Superior), and ANP (Agência Nacional do Petróleo, Gás Natural e Biocombustíveis) is gratefully acknowledged.

References

[1] Abouhamze M, Shakeri M. Multi-objective stacking sequence optimization of laminted cylindrical panels using a genetic algorithm and neural networks. Composite Structures 2007;81:253–63.
[2] ABS. Guide for building and classing subsea riser systems. American Bureau of Shipping; 2006.
[3] Adali S, Verijenko VE, Richter A. Minimum sensitivity design of laminated shells under axial load and external pressure. Composite Structures 2001;54:139–42.
[4] Akbulut M, Sonmes FO. Optimum design of composite laminates for minimum thickness. Computers and Structures 2008; 86:1974–82.
[5] Almeida FS, Awruch AM. Design optimization of composite laminated structures using genetic algorithms and finite element analysis. Composite Structures 2009;88:443–54.
[6] Arora J. In: Introduction to optimum design. 2nd ed. Elsevier; 2004.
[7] Blom AW, Stickler PB, Gurdal Z. Optimization of composite cylinder under bending by tailoring properties in circunferential direction. Composites: Part B 2010;41:157–65.
[8] Chipperfield AJ, Fleming PJ, Pohlheim H, Fonseca CM. Genetic algorithm toolbox user's guide. University of Sheffield; 1994.
[9] Cook RD, Malkus DS, Plesha ME, de Witt RJ. In: Concepts and applications of finite element analysis. 4th ed. John Wiley & Sons; 2002.
[10] Daniel IM, Ishai O. In: Engineering mechanics of composite materials. 2nd ed. Oxford University Press; 2006.
[11] DNV. DNV-OS-F201 – dynamic risers – offshore standard. Det Norske Veritas; 2010.
[12] DNV. DNV-RP-F202 – composite risers – recommended practice. Det Norske Veritas; 2010.
[13] Erdal O, Sonmez FO. Optimum design of composite laminates for maximum buckling load capacity using simulated annealing. Composite Structures 2005;71:45–52.
[14] Goldberg DE. Genetic algorithms in search, optimization and machine leaning. Addison-Wesley; 1989.
[15] Gurdal Z, Haftka RT, Hajela P. Design and optimization of laminated composite materials. Wiley-Interscience; 1999.
[16] Jones RM. In: Mechanics of composite materials. 2nd ed. Taylor & Francis; 1999.
[17] Kim WK. Composite production riser assessment. PhD dissertation. USA: Texas A&M University; 2007.
[18] Larsen CM, Hanson T. Optimization of catenary risers. Journal of Offshore Mechanics and Arctic Engineering 1999;121: 90–4.
[19] Lima BSLP, Jacob BP, Ebecken NFF. A hybrid fuzzy/genetic algorithm for the design of offshore oil production risers. International Journal for Numerical Methods in Engineering 2005;64:1459–82.
[20] MATLAB optimization toolbox™ user's guide. MathWorks, Inc.; 2010.
[21] Meniconi LCM, Reid SR, Soden PD. Preliminary design of composite riser stress joints. Composites Part A: Applied Sciences and Manufacture 2001;32:597–605.
[22] Ochoa OO, Salama MM. Offshore composites: transition barriers to an enabling technology. Composites Science and Technology 2005;65(15, 16):2588–96.
[23] Ochoa OO. Composite riser: experience and design practice, final project report. Offshore Technology Research Center (OTRC), Texas A&M University; 2006.
[24] Odru P, Poirette Y, Stassen Y, Saint-Marcoux JF, Abergel L. Technical and economical evaluation of composite riser systems. in Offshore technology conference, OTC 14017, Houston, TX; May 6–9, 2002.
[25] Pina AA, Albrecht CH, Lima BSLP, Jacob BP. Tailoring the particle swarm optimization algorithm for the design of offshore oil production risers. Optimization and Engineering 2010;12(1, 2):215–35.
[26] Rao ARM, Shyju PP. A meta-heuristic algorithm for multi-objective optimal design of hybrid laminate composite structures. Computer-Aided Civil and Infrastructure Engineering 2010;25:149–70.
[27] Reddy JN. In: Mechanics of laminated composite plates and shells: theory and analysis. 2nd ed. CRC Press; 2004.
[28] Rodriguez DE, Ochoa OO. Flexural response of spoolable composite tubulars: an integrated experimental and computational assessment. Composites Science and Technology 2004;64:2075–88.
[29] Salama MM, Stjern G, Storhaug T, Spencer B, Echtermeyer A. The first offshore field installation for a composite riser joint. In: Offshore technology conference, OTC 14018, Houston, TX; May 6–9, 2002.

[30] Salama MM. Some challenges and innovations for deepwater developments. In: Offshore technology conference, OTC 8455, Houston, TX; May 5–8, 1997.
[31] Shin DK, Gurdal Z, Griffin Jr OH. A penalty approach for nonlinear optimization with discrete design variables. Engineering Optimization 1990;16:29–42.
[32] Smith KL, Leveque ME. Ultra-deepwater production systems final report, Houston, TX; August 2005.
[33] Sparks CP. Fundamentals of marine riser mechanics: basic principles and simplified analysis. PennWell Books; 2007.
[34] Tamarelle PJC, Sparks CP. High-performance composite tubes for offshore applications. In: Offshore technology conference, OTC 5384, Houston, TX; April 27–30, 1987.
[35] Tanaka RL, Martins CA. Parallel dynamic optimization of steel risers. Journal of Offshore Mechanics and Arctic Engineering 2011;133(1). 9 pp.
[36] Teófilo FAF, Parente Jr E, Melo AMC, Holanda AS. Buckling of laminated tubes under external pressure. In: Iberian Latin American congress on computational methods in engineering. Rio de Janeiro: Armação de Búzios; 2009. p. 1–15.
[37] Vieira IN, Lima BSLP, Jacob BP. Optimization of steel catenary risers for offshore oil production using artificial immune system. In: Bentley Peter J, Lee Doheon, Jung Sungwon, editors. ICARIS 2008, lecture notes in computer science 5132 2008. p. 254–65.
[38] Weingarten VI, Seide P, Peterson JP. Buckling of thin-walled circular cylinders, NASA SP-8007, space vehicle design criteria (structures); 1968.
[39] Witz JA. A case study in the cross-section analysis of flexible risers. Marine Structures 1996;9(9):885–904.
[40] Yang H, Jiang R, Li H. Optimization design of deepwater steel catenary risers using genetic algorithm. In: Yuan Yong, Cui Junzhi, Mang Herbert A, editors. Computational structural engineering. Springer; 2009. p. 901–8.